*36th EPS Conference on Plasma Phys. Sofia, June 29 - July 3, 2009 ECA Vol.**33E**, P-4.140 (2009)*

Scaling of Divertor Heat Flux Profile Widths in DIII-D

C.J. Lasnier[1], M.A. Makowski[1], J.A. Boedo[2], N.H. Brooks[3], A.W. Leonard[3], J.G. Watkins[4], and W.P. West[3]

[1]*Lawrence Livermore National Laboratory, Livermore, California, USA*
[2]*University of California-San Diego, La Jolla, California, USA*
[3]*General Atomics, PO Box 85608, San Diego, California 92186-5608, USA*
[4]*Sandia National Laboratories, Albuquerque, New Mexico, USA*

I. Introduction

The width of the divertor heat flux profile $w_{q,div}$ is of great interest in future large tokamaks as well as many present devices. Previous studies examining the parametric dependence of $w_{q,div}$ have arrived at diverse scalings [1] in JET [2], ASDEX-Upgrade [3], JT60-U [4,5], DIII-D [6,7], and NSTX [8] with results somewhat at variance with each other. We attempt here to perform a new series of experiments in DIII-D to obtain scaling of the divertor heat flux peak value, profile width, and divertor plate power as a function of plasma input parameters, with the maximum number of divertor and scrape-off-layer (SOL) diagnostics brought to bear.

We performed measurements in lower single-null edge localized mode (ELM) H-mode diverted configurations that, due to the strike-point positions, were not strongly pumped. We varied the plasma current I_p at constant toroidal field B_T, and varied line-averaged density $\bar{n}_e$ at constant I_p and B_T. The neutral beam injected power P_{inj} was changed at constant I_p and B_T, B_T at constant I_p, and B_T/I_p at constant q_{95}. The divertor heat flux was calculated from infrared camera measurements using a new high-resolution fast-framing IR camera.

The IR camera recorded divertor plate surface thermal emission at multi-kilohertz frame rates through the whole discharge to allow measuring time-averaged data as well as rapid changes due to ELMs. The heat flux at each position in the radial profile was calculated at each of the times steps using the THEODOR 2D heat flux analysis code [9]. We show scaling of the divertor peak heat flux and profile width as a function of the parameters varied, and compare with published results from other devices.

II. Peak Divertor Heat Flux

For each discharge, one or more time intervals of interest were selected where plasma conditions varied little during the interval. The average of each quantity was compiled for each interval. Low-frequency ELMs are included in the average with only small effect.

Figure 1 shows the peak heat flux at the inner (ISP) and outer strike points (OSP) plotted against the input power (neutral beam heating plus Ohmic heating power), where I_p = 1.3 MA, B_T = –1.9 T were held constant. Density was between 5.2 and 6.5×10^{19} m^{-3}, except at the highest power, where $\bar{n}_e = 2.3\times10^{19}$ m^{-3}. Linear fits are shown. A linear dependence of peak heat flux on input power can reasonably be concluded, with the caveat that not all points were taken at the same density. Without the highest power point, we still see a linear dependence.

Figure 2 again shows peak heat flux at the ISP and OSP, this time plotted against line-averaged density, where P_{inj} = 4.6–4.7 MW except for the densities $\bar{n}_e$ = 5.2×10^{19} m^{-3}, where P_{inj} = 7 MW, and $\bar{n}_e$ = 6.8×10^{19} m^{-3} where P_{inj} = 3.8 MW. Toroidal field was held constant at B_T = –1.9 T, and plasma current was held at I_p = 1.3 MA. Linear fits to the data are shown. If the two density values where P_{inj} varied are eliminated, the dependence of peak heat flux on density still is linear.

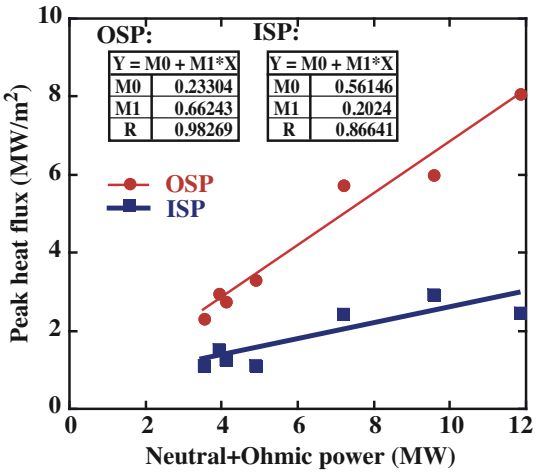

Fig. 1. Peak heat flux at the ISP and OSP plotted against the input power. Linear fits to the data are plotted, with fitting parameters shown in the boxes.

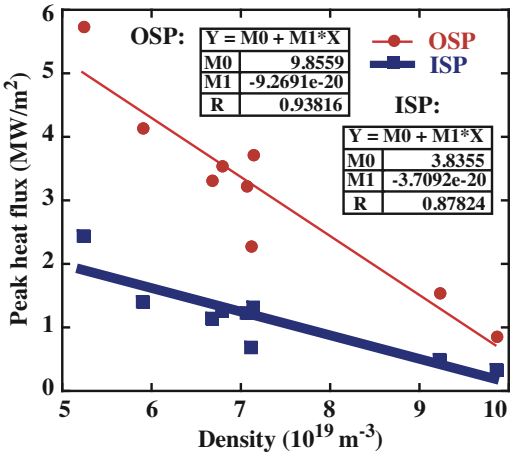

Fig. 2. Peak heat flux at the ISP and OSP plotted against line-averaged density.

Figure 3 depicts the peak heat fluxes, now plotted against plasma current, showing a linear dependence. Toroidal field was held at B_T = –1.9 T, and P_{inj} = 4.65–4.8 MW except for the point at I_p = 1.3 MA where P_{inj} = 3.8 MW. Density was not held constant, but allowed to vary at the natural H-mode density, because of practical difficulty measuring the heat flux at the OSP during the plasma pumping that would have been required to maintain constant density. Figure 4 shows the density variation during the I_p scan. Because of the density variation in this set, this plot does not prove the variation with I_p alone. In combination with the density scan at constant I_p, the dependence on I_p will be extracted from a multi-parameter fit to a larger data set in a later analysis.

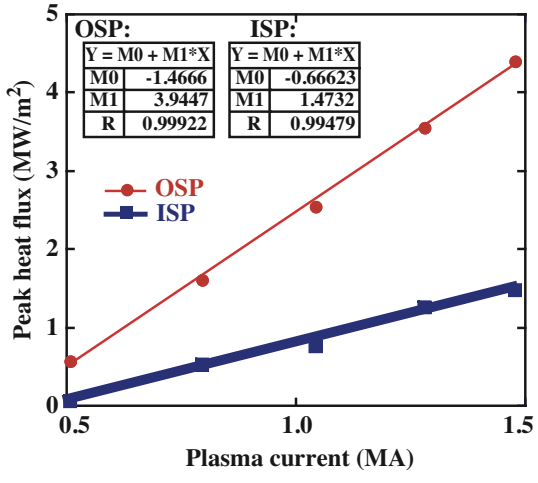

Fig. 3. Peak heat fluxes, now plotted vs. I_p.

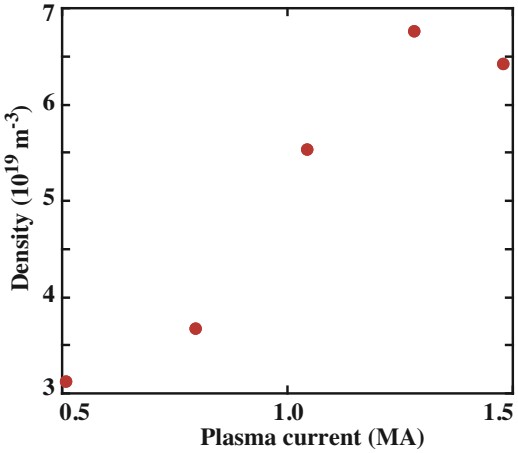

Fig. 4. Density variation during the I_p scan.

Figure 5 shows peak heat fluxes plotted against B_T at nearly constant safety factor q_{95} = 3.6–3.7, with linear fits. Density ranged from $\bar{n}_e$ = 3.2×10^{19} m^{-3} at the lowest field to $\bar{n}_e$ = 5.8×10^{19} m^{-3} at the highest field. There are not enough data points to conclusively show a linear dependence, but that would be consistent with the data. Since we know from Fig. 2 that the peak heat flux decreases with increasing density, this indicates that if density were held constant, the heat flux would increase faster than linearly with increasing toroidal field magnitude at constant q_{95}.

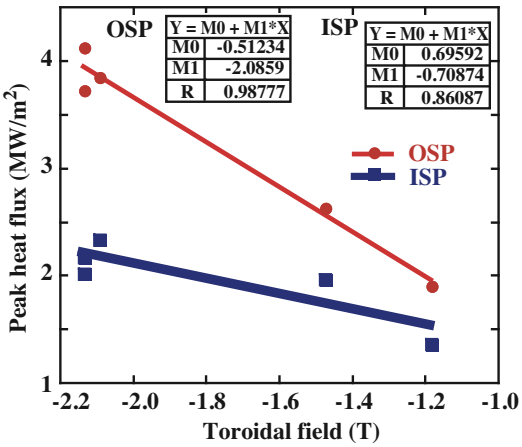

Fig. 5. Peak heat fluxes plotted against B_T at nearly constant safety factor.

III. Heat Flux Profile Width

Profile widths discussed here are full width at half maximum (FWHM) values for the ISP and OSP respectively. Widths are obtained at each time point and averaged over the time intervals of interest. Here $w_{q,div}$ shows no dependence on input power (not shown).

Figure 6 shows the outer and inner $w_{q,div}$ plotted against density, for the same density scan as above. There is no effect at low density, but there is a threshold density where the profile becomes wider.

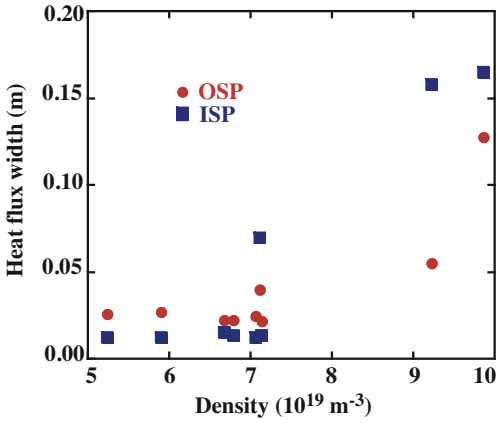

Fig. 6. OSP and ISP heat flux profile widths plotted against density.

In Fig. 7 is seen $w_{q,div}$ plotted against I_p, for the current scan already described. We see that widths become larger at low current. The fitted curve for the ISP is linear, but for the OSP, a better fit goes inversely as nearly the first power of the plasma current. No ISP heat flux peak was seen at the lowest I_p. We expect the current dependence of the inner width would be of a similar functional form to that of the OSP if more data were available. In Fig. 3, the peak heat flux for this case at the ISP is very small.

The plot in Fig. 8 shows $w_{q,div}$ versus toroidal field at constant q_{95} for the same discharges as described for the peak heat flux scaling. The widths decrease linearly with the magnitude of the toroidal field.

IV. Comparisons With Other Empirical Scalings

Loarte summarized several empirical scalings in Ref. 1, pointing out the areas of disagreement. Here we compare the functional dependences seen above with those scalings.

The linear dependence on power seen above is in agreement with the JET, ASDEX-Upgrade (DIVIII), and previous DIII-D scaling, but not the ASDEX-U (DIVI) scaling. We

note that several of those studies use divertor or target power rather than input power. We find the same linear correlation of peak heat flux with target power as with input power.

We have not observed a clear dependence of peak heat flux on toroidal field at fixed I_p in the present data, unlike the previous DIII-D study which found a variation of $1/B_T^{0.5}$. The linear increase in peak heat flux with I_p peak agrees with the previous DIII-D result.

The $w_{q,div}$ we use here is different than the λ_q of the referenced studies, which defined an effective width by dividing the strike point power by the peak heat flux. We find in agreement with NSTX, JET IR and ASDEX-Upgrade (DIVII), essentially no (or very weak) dependence of the width on power. We find in agreement with NSTX that the width decreases with increasing plasma current, approximately as $1/I_p$.

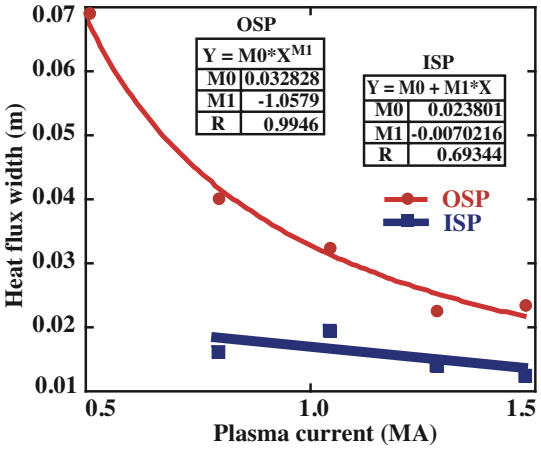

Fig. 7. Profile widths plotted against plasma current.

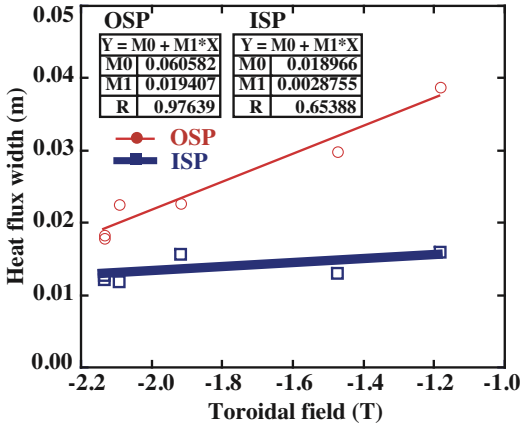

Fig. 8. Profile widths versus toroidal field at constant q_{95}.

V. Conclusion

In the present study we find that peak heat flux varies linearly with input power, inversely as density, linearly with plasma current with a caveat that density was not fixed, and linearly with the magnitude of the toroidal field with q_{95} held constant.

We find FWHM $w_{q,div}$ depends not at all on power, and not on density at low density. There is a density threshold for profile broadening. We see $w_{q,div}$ varies inversely with the I_p and decreases linearly with increasing B_T at constant q_{95}. This is the opposite direction of the dependence on I_p, so this is not simply due to the increase in I_p.

We expect to examine this data set further with other fitting techniques as well as making a study of the ELM heat flux profiles from the parameter scans above.

This work was supported by the US Department of Energy under DE-AC52-07NA27344, DE-FG02-07ER54917, DE-FC02-04ER54698, and DE-AC04-94AL85000.

References

[1] A. Loarte, *et al.*, Nucl Fusion **47**, S203 (2007).
[2] T. Eich, *et al.*, J. Nucl. Mater. **333–339**, 669 (2005).
[3] A. Herrmann, Plasma Phys. Control. Fusion **44**, 883 (2002).
[4] ITER Physics Basis Editors, Nucl. Fusion **39**, 2137 (1999).
[5] A. Loarte, *et al.*, J. Nucl. Mater. **266–269**, 587 (1999).
[6] D.N. Hill, *et al.*, J. Nucl. Mater. **196–198**, 204 (1992).
[7] C.J. Lasnier, *et al.*, Nucl. Fusion **38**, 1225 (1998).
[8] R. Maingi, *et al.*, J. Nucl. Mater. **363–365**, 196 (2007).
[9] A. Herrmann, *et al.*, Plasma Phys. Control. Fusion **37,** 17 (1995).